Chinese Journal of
POLYMER SCIENCE

RESEARCH ARTICLE

https://doi.org/10.1007/s10118-026-3616-7
Chinese J. Polym. Sci. **2026**, *44*, 1830–1842

Hysteresis-free and Fatigue-resistant Conductive Hydrogel Electronics towards Intelligent Human-machine Interaction

Liu-Yu Zhang[a,b,†], Gen Li[b,†], Gui-Neng Li[b], Yu-Zhu Hou[c], Hua Li[a*], Yu Xue[b,e*], Wei-Jing Zhao[d*], and Bao-Yang Lu[b,e*]

[a] *Jiangxi Provincial Key Laboratory of Immunology and Inflammation, Jiangxi Provincial Clinical Research Center for Laboratory Medicine, Health Management Center, The Second Affiliated Hospital, Jiangxi Medical College, Nanchang University, Nanchang 330006, China*
[b] *Jiangxi Provincial Key Laboratory of Flexible Electronics, Flexible Electronics Innovation Institute, Jiangxi Science and Technology Normal University, Nanchang 330013, China*
[c] *College of Information Engineering, Jiangxi Science and Technology Normal University, Nanchang 330013, China*
[d] *Department of Endocrinology and Metabolism, Shanghai Sixth People's Hospital Affiliated to Shanghai Jiao Tong University School of Medicine; Shanghai Clinical Center for Diabetes; Shanghai Key Clinical Center for Metabolic Disease; Shanghai Diabetes Institute; Shanghai Key Laboratory of Diabetes Mellitus, Shanghai 200233, China*
[e] *Institute of Energy Materials and Nanotechnology, Nanchang Jiaotong Institute, Nanchang 330100, China*

Electronic Supplementary Information

Abstract Conductive hydrogel-based strain sensors, as key components of electronic skins, have garnered significant attention for the development of advanced human-machine interfaces and flexible electronics. However, their intrinsic limitations of large hysteresis and poor mechanical robustness pose significant challenges for achieving the high accuracy and long-term stability required for advanced sensing systems. Here, we achieve hysteresis suppression and structural stability by constructing a microphase-separated interlocking network within a 3D-printable poly(vinyl alcohol) (PVA)/conductive carbon black (CCB) hydrogel. The resulting conductive hydrogel strain sensor possesses low electrical hysteresis (0.82%) and high cycle stability (>1×10^4 cycles), enabling real-time and precise monitoring of joint bending and muscle contraction. By converting finger motion into machine-learnable signal patterns, the sensor enables an identification system that decodes continuous strain signals into alphabetical information, offering a novel human-machine interaction modality. This work provides a promising conductive hydrogel platform with enhanced sensing fidelity and interaction capability towards intelligent human-machine interactions.

Keywords Conductive hydrogel; Strain sensors; Hysteresis-free; Fatigue-resistant; Intelligent interactive systems

Citation: Zhang, L. Y.; Li, G.; Li, G. N.; Hou, Y. Z.; Li, H.; Xue, Y.; Zhao, W. J.; Lu, B. Y. Hysteresis-free and fatigue-resistant conductive hydrogel electronics towards intelligent human-machine interaction. *Chinese J. Polym. Sci.* **2026**, *44*, 1830–1842.

INTRODUCTION

Human-machine interfaces (HMIs) enable efficient bidirectional communication *via* devices such as smartphones and touchpads, revolutionizing interaction modalities and serving as key components across domains ranging from industrial automation to consumer electronics.[1–3] As core elements within interactive systems, flexible strain sensors attract broad interest in HMI applications because they seamlessly integrate with the skin and transduce mechanical stimuli into electrical signals. Although flexible sensors based on elastomers,[4,5] conductive nanomaterials,[6–8] and liquid metals continue to advance,[9–11] conductive hydrogel strain sensors are highly promising candidates owing to their combined advantages of high stretchability, softness, and biocompatibility.[12–15] However, a primary limitation is mechanical hysteresis: during repeated stretching, energy dissipation accumulates and progressively degrades the accuracy and stability of the output signals.[16,17]

Recent efforts focus on designing conductive hydrogels with low mechanical hysteresis by regulating the energy dissipation and recovery within polymer networks.[18–20] A common strategy introduces dynamic and reversible crosslinks (*e.g.*, borate ester bonds and metal-ligand coordination), which break under load to dissipate energy and reform upon unloading to restore the structure.[21–23] However, under high-frequency or large-strain cyclic motion (such as continuous finger bending or joint flexion-extension), hysteresis increases, causing strain-signal drift and inaccurate motion tracking. In addition, by constructing composite networks where distinct components offer elastic support and dissi-

* Corresponding authors, E-mail: ndefy00059@ncu.edu.cn (H.L.)
E-mail: xueyu8@jxstnu.edu.cn (Y.X.)
E-mail: z811wj@163.com (W.J.Z.)
E-mail: luby@jxstnu.edu.cn (B.Y.L.)
† These authors contributed equally to this work.
Received December 3, 2025; Accepted February 5, 2026; Published online May 9, 2026

pate energy, decoupling between low-energy dissipation and fast recovery is achieved.[24–26] However, such systems often rely on complex structural designs or demanding polymerization conditions, and certain dynamic bond motifs or multinetwork systems exhibit pronounced fatigue after repeated cycles, making it difficult to balance low hysteresis with structural robustness.[27,28] Therefore, there is an urgent need for a structurally simple, yet highly effective design strategy that can achieve a balanced combination of stable energy dissipation and mechanical robustness.

To address these challenges, we propose a strategy based on constructing a microphase-separated interlocking network that leverages the synergistic integration of conductive fillers within an elastic matrix. PVA forms a physically crosslinked matrix *via* freeze-thaw-induced crystallites and a hydrogen-bond network, providing recoverable structural support. CCB serves as a functional filler that establishes a continuous conductive network while strengthening interchain coupling and stress transfer through interfacial hydrogen bonding and physical adsorption. This multiscale synergy creates hierarchical dissipation pathways at the microscopic level and enables low-hysteresis, high-durability, mechanoelectrical transduction at the macroscopic level. Thus, PVA/CCB hydrogel sensors convert mechanical strain into stable, discernible electrical outputs. We further integrate a machine-learning-assisted human-machine interface, which demonstrates a systematic route from structural regulation and stable conduction to intelligent recognition and provides new material and architectural concepts for reliable conductive hydrogels aimed at wearable and cognitive interaction applications.

MATERIALS AND METHODS

Materials

Poly(vinyl alcohol) (PVA; M_w = (1.24×10^5–1.86×10^5) Da, Sigma-Aldrich), conductive carbon black nanoparticles (CCB; average primary particle size 30–45 nm, XFNANO), and Sylgard 184 silicone elastomer (polydimethylsiloxane, PDMS; catalog no. 0008912877, Dow Corning) with a curing agent (catalog no. H052J9A063; Dow Corning) were purchased and used as received without further purification. All experiments were conducted using Milli-Q ultrapure water.

Preparation of Hydrogel Inks

A 10 wt% PVA solution was prepared by dissolving 10 g of PVA powder in 90 g of deionized water, followed by stirring at 90 °C for 2 h until complete dissolution. Separately, a 1 wt% CCB dispersion was obtained by adding 0.1 g of CCB to 9.9 g of deionized water, which was then vigorously stirred and subsequently ultrasonicated for 30 min to achieve a homogeneous suspension. The PVA solution and CCB dispersion were then mixed in specific mass ratios to formulate a series of PVA/CCB inks. The CCB contents were set to 1 wt%, 5 wt%, 10 wt%, and 20 wt%, calculated as the mass of CCB divided by the combined mass of PVA and CCB solids. The mixtures were degassed *via* centrifugation at 5000 r·min^{-1} for 30 min, yielding homogeneous, 3D-printable PVA/CCB inks.

3D Printing and Formation of Hydrogels

The rheological properties of the PVA/CCB hydrogel precursor inks were characterized using a Discovery Hybrid Rheometer (TA Instruments, USA) at 20 °C with a 4 mm parallel-plate geometry. The shear rate ranged from 0 s^{-1} to 400 s^{-1} to evaluate the shear-thinning behavior and printability.

Printing geometries were designed in Adobe Illustrator 2019, saved as SVG files, and imported into the DB-100 3D printer (Shanghai Mifang Electronics Technology Co., Ltd.) software for model adjustment and tool-path planning. The nozzle diameter, pneumatic pressure, and printing speed were optimized. The printed hydrogel precursors subsequently underwent three freeze-thaw cycles (freezing at –20 °C for 8 h and thawing at 20 °C for 2 h per cycle), which yielded PVA/CCB conductive hydrogels with enhanced mechanical performance and sensing functionality. The PDMS curing agent was mixed with the PDMS precursor solution at a mass ratio of 1:10, followed by mechanical stirring for 30 min and centrifugation to remove trapped air, yielding a homogeneous PDMS ink. The prepared ink was used to print the substrate and encapsulation layers of the device. To prevent premature curing, the PDMS ink was prepared immediately before use.

Mechanical and Electrical Properties

Mechanical properties were measured on a microcomputer-controlled universal testing machine (ZQ-990LB, Zhiqu Precision Instruments). The sample width and gauge length were measured using a Vernier caliper, and the thickness was determined using a micrometer screw gauge. Each specimen was clamped in a tensile grip to ensure alignment between the central axis of the specimen and the loading direction. Electrical properties were characterized using a precision LCR meter (TH2829C, Tonghui; 20 Hz–1 kHz) in a four-probe configuration. During testing, the electrode probes were brought into firm contact with the two ends of the specimen to ensure low contact impedance. The electrical conductivity (σ) was calculated using the following equation:

$$\sigma = L/(R \cdot W \cdot T) \tag{1}$$

where L, R, W, and T denote the length (m), resistance (Ω), width (m), and thickness (m) of the sample, respectively.

Sensing Performance

The PVA/CCB hydrogel sample was mounted on a universal testing machine, with both ends connected to an LCR meter *via* conductive carbon cloth. Based on the integrated area of the resistance versus strain curves obtained during the loading and unloading processes, the electrical hysteresis (H) was calculated using the following equation:

$$H = \left(1 - \frac{A_2}{A_1}\right) \times 100\% \tag{2}$$

where H represents the hysteresis (%), and A_1 and A_2 denote the areas of the loading (increasing segment of the resistance-strain curve) and unloading (decreasing segment of the resistance-strain curve) processes, respectively.

To further investigate the strain-sensing performance of the hydrogel, an LCR meter was used to monitor the real-time resistance changes in the sample under different applied strains. By analyzing the relationship between the relative resistance change and applied strain, the sensitivity of the hydrogel sensor, defined as the gauge factor (GF), was calculat-

ed using the following equation:

$$GF = \frac{\Delta R}{R_0 \cdot \varepsilon} \quad (3)$$

where GF represents the gauge factor, ΔR is the change in resistance, R_0 is the initial resistance, and ε is the applied strain, respectively.

To evaluate the cyclic stability of the sample, multiple loading-unloading tests were conducted at a stretching rate of 500 mm/min, and the variations in each cycle were recorded in real time.

Machine Learning Modeling and Performance Evaluation

The machine learning network was trained using the TensorFlow framework for experimental data modeling and performance prediction. The experimental environment was based on an Ubuntu 18.04 operating system, equipped with an NVIDIA GeForce RTX 3080 Ti GPU. The input data were one-dimensional signals that were normalized and subjected to feature extraction before being fed into a three-layer neural network model. To guarantee reproducibility, we employed a fixed random seed to randomly split the dataset into training (80%) and validation (20%) subsets. The validation set was leveraged during training for progress monitoring and early stopping. Parameter updates were performed using mini-batch training, with a consistent batch size of 32. The network weights were optimized using the backpropagation algorithm to minimize the mean squared error loss function, and dropout and early stopping strategies were applied to prevent overfitting. After training, the model performance was evaluated using the test dataset. The accuracy curves of the training and validation stages were plotted to analyze the convergence behavior, and a confusion matrix was calculated to assess the classification accuracy and error distribution, thereby verifying the stability and generalization capability of the model.

RESULTS AND DISCUSSION

Design of High-performance Hydrogel Strain Sensors

Reliable human-machine interactions are underpinned by high-performance hydrogel strain sensors operating in concert with advanced algorithms. However, conventional hydrogel sensors are often plagued by signal hysteresis, compromising their reliability as core components in human-machine interfaces. The hydrogel sensor we develop shows low hysteresis, ensuring that its electrical output faithfully reflects the instantaneous mechanical state of the material, thereby establishing an efficient information interaction platform (Fig. 1a). PVA serves as a hydrogel matrix, providing a robust and biocompatible framework.[29–31] Concurrently, CCB is introduced as a nanofiller to establish continuous electron transport pathways within the composite, which are essential for achieving reliable and stable signal transmission.[32,33]

To meet the demand for high-performance strain sensors in diverse applications, 3D printing is employed for the customized fabrication of PVA/CCB hydrogel sensors, enabling precise geometric control and complex architectures. Notably, 3D printing induces an ordered alignment of molecular chains and fillers along the printing path, which further optimizes the continuity of the conductive network and enhances the stress transfer efficiency. The printed constructs are subsequently subjected to cyclic freeze-thaw processing to engineer a multilevel cooperative network. This post-printing treatment induces the formation of crystallite domains, a dense hydrogen-bond network, and interchain entanglements (Fig. 1b). At low temperatures, PVA chains reorganize into crystallites that serve as robust physical crosslinks, significantly reinforcing the network integrity.[34–36] Meanwhile, hydrogen bonds function as reversible sacrificial bonds that dissociate under applied strain to dissipate energy and alleviate stress concentration, and then reversibly reform during unloading to restore the structure. Simultaneously, chain entanglements provide flexible topological constraints that restrict chain slippage and facilitate shape recovery, thereby synergistically enhancing the cyclic stability and markedly reducing the hysteresis loss. The incorporation of CCB endows the system with electrical conductivity and improves mechanical robustness through nano-reinforcement effects. CCB interacts with the PVA chains *via* hydrogen bonding and electrostatic interactions, stabilizing the conductive network and maintaining pathway continuity during deformation. Uniform dispersion of nanoscale CCB enables efficient load transfer and mitigates stress concentration while cooperatively interacting with crystallite domains and hydrogen bonds to construct a microphase-separated interlocking network. As illustrated in Fig. 1(c), conventional covalently crosslinked conductive hydrogels often exhibit pronounced electromechanical hysteresis during cyclic stretching-release owing to long chain segments between crosslinking points and the asynchronous responses of mechanical and conductive networks. In contrast, the microphase-separated interlocking network in this work promotes synchronized mechanical deformation and conductive pathway evolution, thereby achieving low hysteresis and high cyclic stability.

3D Printing of PVA/CCB Hydrogels

The excellent dispersibility of the CCB within the PVA matrix provides a crucial foundation for the formulation of 3D-printable inks. To determine the optimal composition, we systematically evaluate the appearance and dispersion state of inks with varying CCB loadings (Fig. 2a). Although increasing the CCB content enhances the electrical conductivity, excessive filler densifies the polymer network and compromises extensibility, whereas an inadequate amount fails to establish continuous conductive pathways. Therefore, the ink with 10 wt% CCB is chosen as the optimal formulation for printing. This optimized ink demonstrates pronounced shear-thinning behavior, where the viscosity decreases significantly with increasing shear rate (Fig. S1 in the electronic supplementary information, ESI). The reduced viscosity enables smooth extrusion, whereas rapid viscosity recovery after the cessation of shear prevents collapse and sustains the stability of printed architectures.[37,38] In addition, both the storage modulus (G') and loss modulus (G'') increase with angular frequency (Fig. S2 in ESI), with G'' remaining slightly higher than G', indicating favorable flowability under low shear, together with sufficient viscoelastic support to satisfy the DIW forming requirements.[39,40]

We systematically evaluate the key DIW parameters, including nozzle diameter, pneumatic pressure, and printing speed, to establish the optimal printing regime. It is found that an insufficient nozzle diameter (60 μm) or pressure (40 kPa) causes nozzle clogging, whereas excessive values result in signifi-

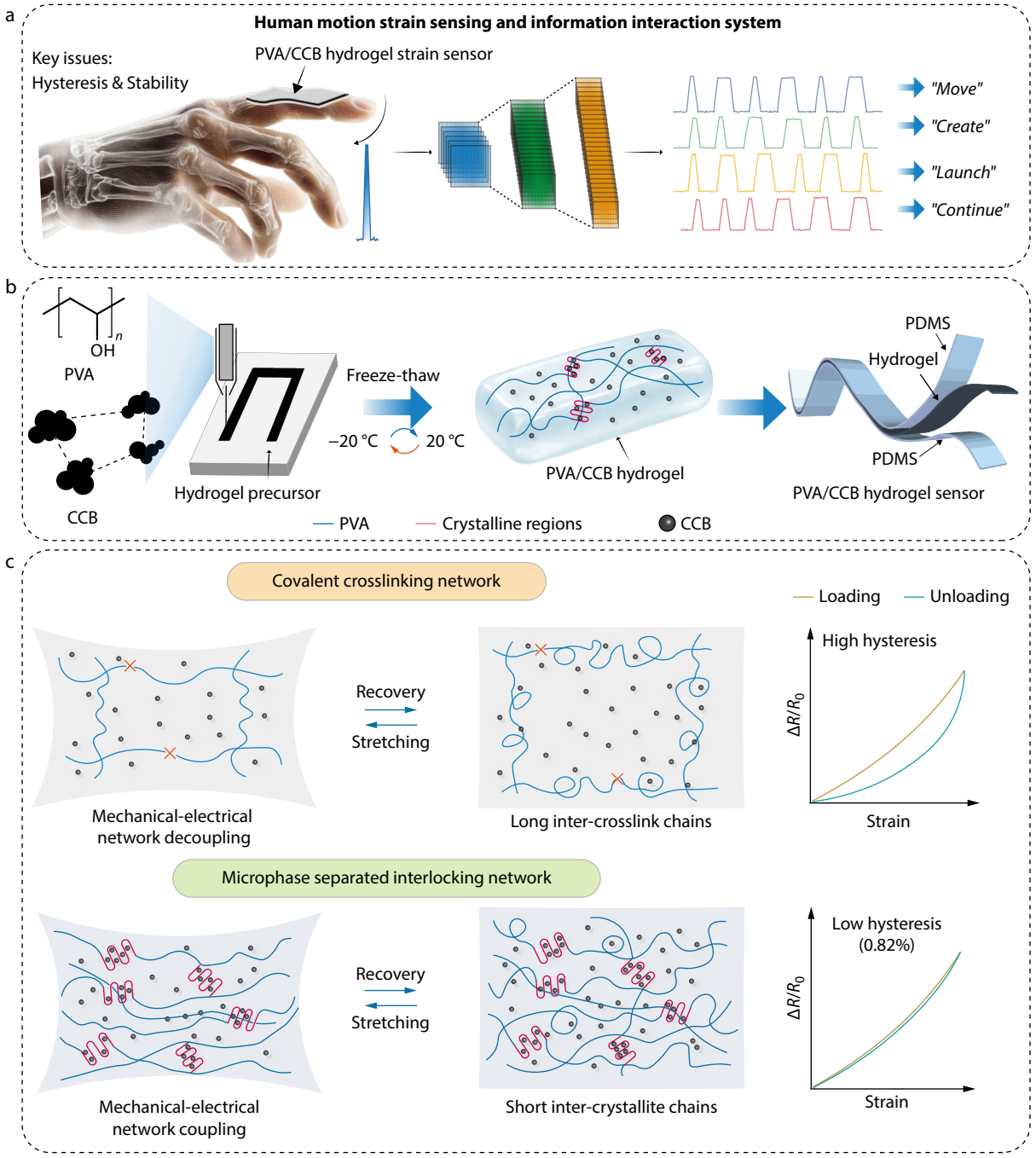

Fig. 1 Design of hysteresis-free and fatigue-resistant conductive hydrogel electronics for intelligent human-machine interaction. (a) Strain-to-information transduction system of the PVA/CCB hydrogel sensor; (b) Schematic illustration of the preparation of PVA/CCB hydrogel strain sensors using 3D printing and freeze-thawing methods; (c) Schematic illustration of the microphase-separated interlocking network enabling low hysteresis and high stability in the PVA/CCB hydrogel sensor.

cant linewidth drift. Optimal extrusion stability and reliability are achieved with a 160 μm nozzle, which operates consistently over the widest operational pressure window (Fig. 2b). Furthermore, at a fixed printing speed of 6 mm·s^{-1}, the applied pressure serves as an effective control parameter for tuning the printed linewidth (Fig. 2c and Fig. S3 in ESI), thereby enabling precise dimensional control (Fig. S4 in ESI).

The shear flow generated during the printing process induces the orientation of the PVA chain segments and CCB fillers along the printing path, thereby forming continuous conductive networks. This structural arrangement imparts lower hysteresis and superior cyclic stability to the material.[41,42] Adopting a forward-printing strategy aligns the strain direction with the printing trajectory, which mitigates the stress concentration and maintains the continuity of the conductive pathways.[43–45] Using this approach under optimized parameters, rectangular and U-shaped hydrogels are obtained with uniform, continuous filaments and sharp inter-

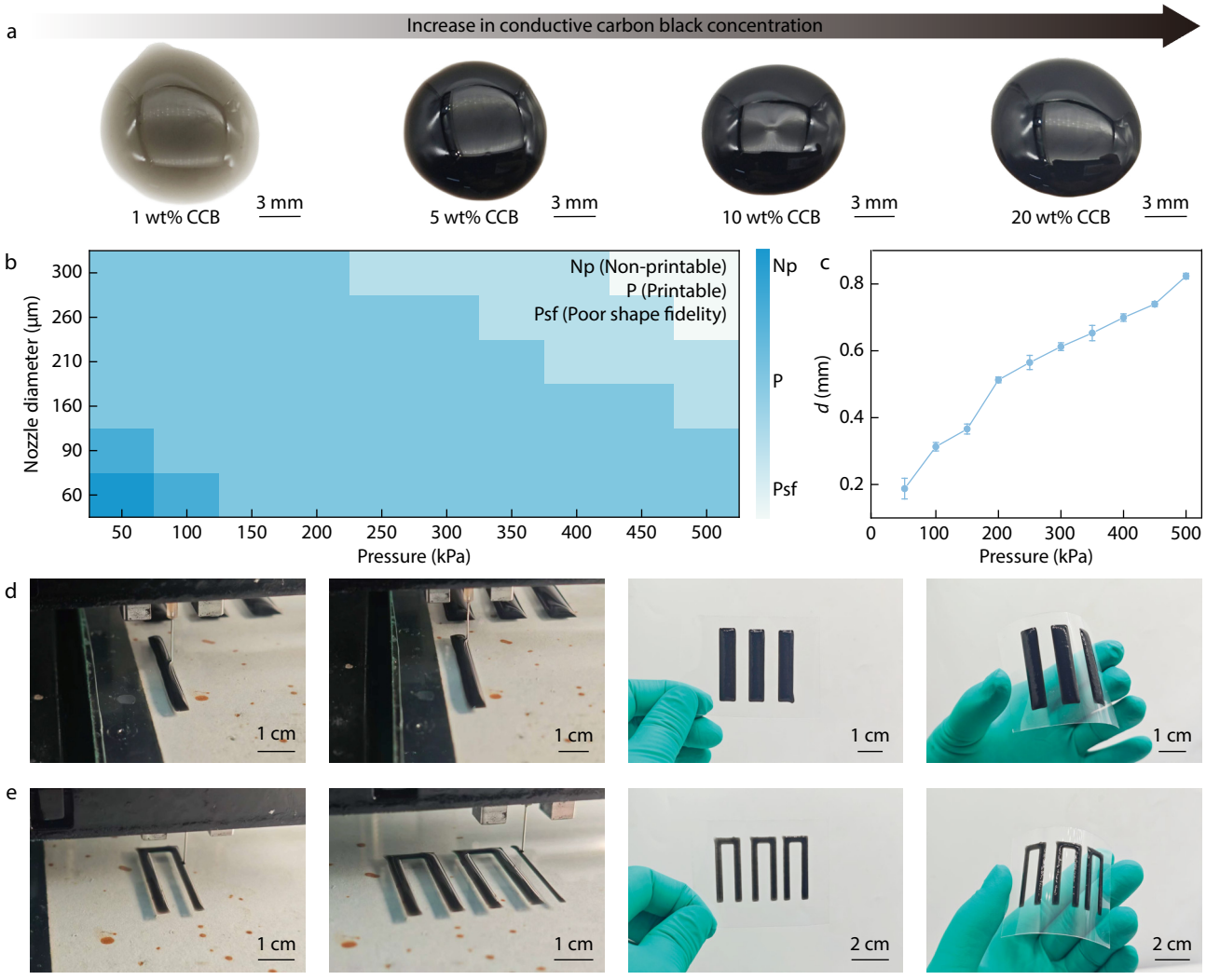

Fig. 2 Evaluation of the 3D printability of PVA/CCB ink. (a) Photographs of PVA/CCB inks with four different CCB concentrations; (b) Printability of PVA/CCB ink using different nozzle sizes and printing pressures; (c) Schematic diagram of line widths obtained using a 160 μm nozzle under different air pressures; (d, e) Printing process and actual demonstration of rectangular and U-shaped hydrogel films.

faces (Figs. 2d and 2e). Their exceptional structural integrity is confirmed by the absence of cracks or delamination after freeze-thaw cycles and bending. Consequently, PVA/CCB (10 wt%) ink, with its synergistic shear-thinning and rapid recovery properties, provides a complete DIW solution for high-fidelity shaping and continuous fabrication, creating a robust platform for developing stable, low-hysteresis flexible sensors.

Mechanical and Electrical Properties of PVA/CCB Hydrogel

PVA/CCB hydrogels exhibit excellent compliance and stable electrical conductivity under mechanical deformation, indicating their potential as core sensing layers in flexible strain-sensing systems. The CCB content exerts a significant regulatory effect on the mechanical properties of PVA/CCB hydrogels (Fig. 3a). The structure of the pure PVA hydrogel is maintained by crystalline domains and hydrogen bonding, resulting in high stiffness but limited extensibility. As the CCB content increases, interfacial interactions arise between the filler particles and PVA chains, generating additional physical crosslinking points and promoting stress dispersion during deformation, thereby enhancing the deformation adaptability. When the CCB content reaches 10 wt%, the strain capacity achieves its optimum value, with a fracture strain as high as 482% (Fig. 3b). However, when the CCB content is further increased to 20 wt%, nanoparticle aggregation readily occurs, leading to local stress concentration and network disruption, which significantly reduces extensibility. These findings indicate that an appropriate amount of CCB not only acts as a stress transfer node but also participates in energy dissipation, serving as a key factor in constructing a compliant and robust network.

With increasing CCB content, the Young's modulus drops to approximately 32 kPa, which is comparable to that of soft skin tissue, following a general decreasing trend with increasing filler loading (Fig. 3c). This compliant characteristic ensures good conformability and signal stability and effectively mitigates the interfacial slippage induced by external motion. Both toughness and fracture strength decrease at higher filler ratios (Figs. 3d and 3e), whereas their variations remain relatively small within the range of 1 wt%–10 wt%, indicating

https://doi.org/10.1007/s10118-026-3616-7

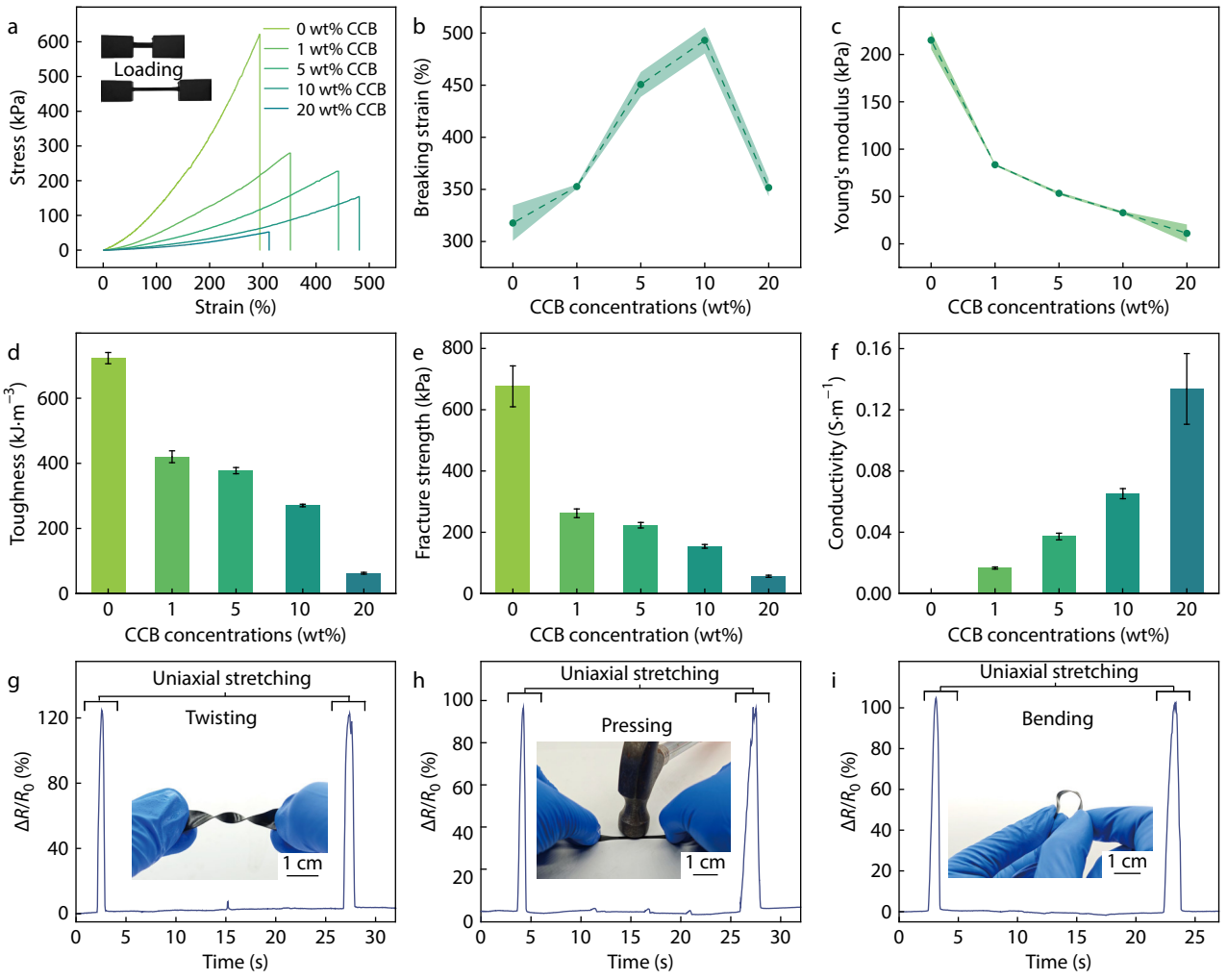

Fig. 3 Mechanical and electrical properties of PVA/CCB hydrogels with different CCB concentrations. (a) Stress-strain curves of PVA/CCB hydrogels with varying CCB concentrations; (b) Breaking strain; (c) Young's modulus; (d) Toughness; (e) Fracture strength; (f) Conductivity; (g, h, i) Resistance responses of the PVA/CCB hydrogel sensor under torsion, compression, and bending.

that a moderate amount of CCB does not compromise the overall mechanical strength. Meanwhile, the multiscale crosslinking formed through the freeze-thaw process provides compensatory reinforcement to the network. Overall, an appropriate CCB content achieves a dynamic balance between the compliance and load-bearing capacity, ensuring both deformability and structural integrity.

The electrical conductivity increases with increasing CCB content, reaching 0.065 and 0.134 S·m^{-1} for 10 wt% and 20 wt%, respectively (Fig. 3f). A stable percolation pathway is established using 10 wt% CCB, enabling the network to maintain electrical continuity under deformation while avoiding the brittleness and interfacial energy dissipation typical of higher filler concentrations. This mechanically and electrically coupled network suppresses irreversible chain slippage and interfacial friction during cyclic loading, thereby reducing hysteresis and improving the signal linearity and stability. In uniaxial tensile tests, the resistance increases rapidly with strain, indicating that deformation stretches or partially disrupts the conductive pathways. In contrast, twisting, pressing, and bending induce only minor fluctuations, demonstrating that the network is highly sensitive to strain direction and exhibits strong anti-interference capability (Figs. 3g–3i). Considering the combined mechanical and electrical performance, as well as the compatibility with 3D printing, subsequent studies focus primarily on PVA/CCB hydrogels with a CCB content of 10 wt%.

Sensing Performance of PVA/CCB Hydrogel

To assess the sensor's potential for wearable electronics, we fabricate a flexible strain sensor by encapsulating a 3D-printed PVA/CCB hydrogel between two thin PDMS films (Fig. 4a). The sensitivity profile of the sensor exhibits three distinct linear regimes, with gauge factors (GF) of 0.69 (0%–100% strain), 1.06 (100%–200%), and 1.62 (200%–300%), and the linear fitting of all three regimes yields R^2 values of approximately 0.997 (Fig. 4b). This segmented response enables discernible signal variations under small deformations and maintains a stable signal response at larger strains, thereby satisfying the wide dynamic range requirements of wearable monitoring systems. During the rapid loading-unloading cycles, the sensor demonstrates a response time of 162.75 ms and a recovery time of 57.33 ms (Fig. 4c). Such rapid response and recovery behaviors indicate that the conductive network can undergo swift structural ad-

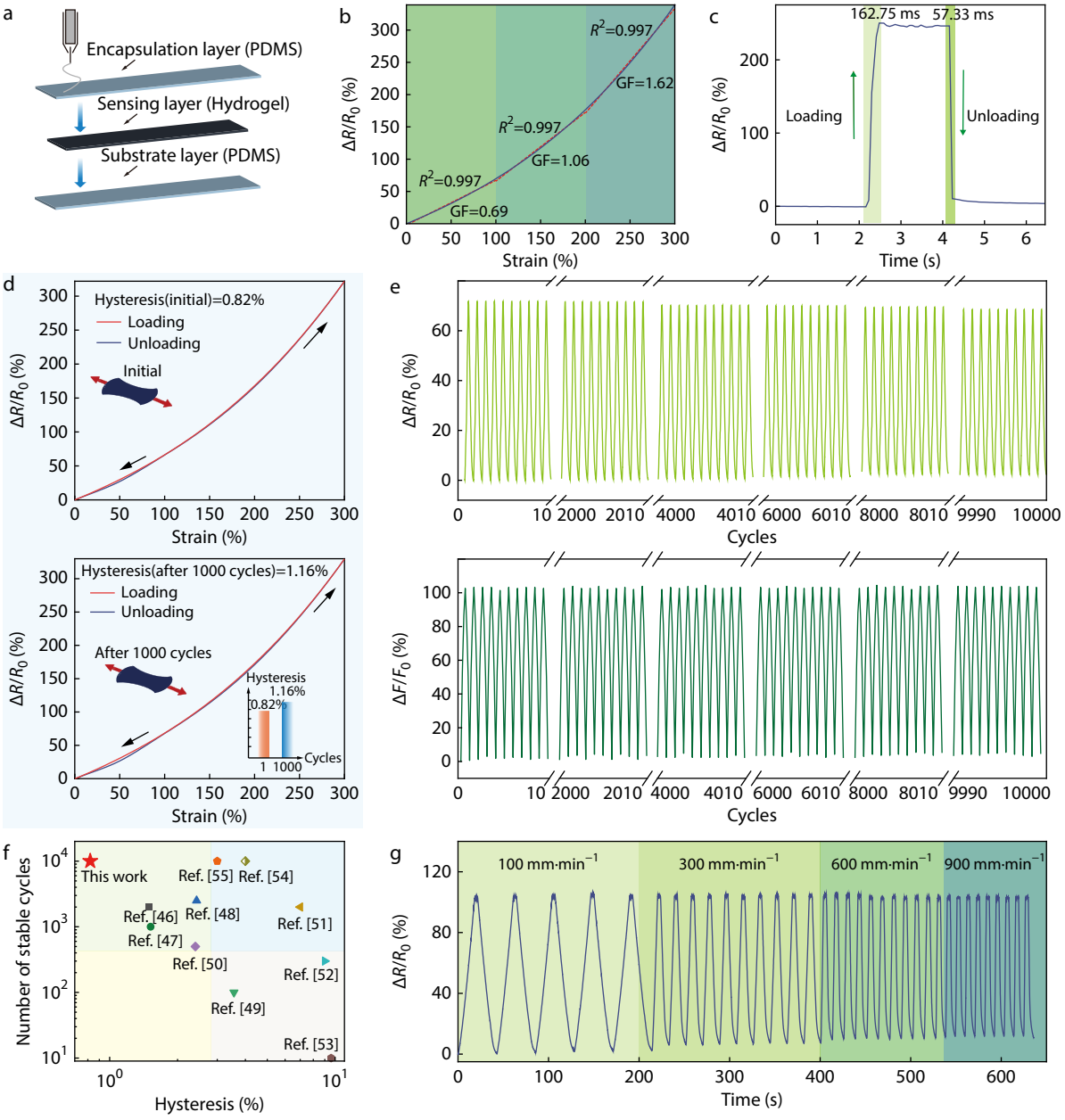

Fig. 4 Sensing performance of the PVA/CCB hydrogel. (a) The PVA/CCB hydrogel is encapsulated with PDMS as a strain sensor; (b) Sensitivity (GF) under different strain ranges, with linear fits and corresponding R^2 values; (c) Response and recovery times under 0%–200% strain; (d) Hysteresis behavior of the PVA/CCB hydrogel at 300% strain and after 1000 stretching cycles; (e) Relative resistance and stress responses during 1×10^4 cyclic stretching-releasing tests at 100% strain; (f) Comparison between the PVA/CCB hydrogel sensor and existing strain sensors; (g) Resistance variation of the PVA/CCB hydrogel under motions at different frequencies.

justments upon the application and release of deformation.

The hydrogel sensor demonstrates exceptional cyclic stability with ultralow hysteresis. The hysteresis ratio remains as low as 0.82% in the initial cycle and shows only a minimal increase to 1.16% after 1000 cycles (Fig. 4d). In addition, outstanding operational durability is confirmed by tests at a tensile speed of 500 mm·min^{-1}, which show negligible drift in both resistance and stress over 1×10^4 cycles at 100% strain (Fig. 4e). Benchmarking against existing hydrogel sensors reveals that our design achieves a superior combination of low hysteresis and robust cyclic stability (Table S1 in ESI). This performance advantage is demonstrated in Fig. 4(f).[46–55] This advantage is governed by a rationally designed structural hierarchy for energy dissipation, where reversible hydrogen bonds serve as sacrificial elements to dissipate local stress, crystallites function as persistent crosslinking sites, and 3D printing-induced chain orientation maintains long-range conductivity. These features operate synergistically to inhibit the irreversible deformation and energy loss.

For segmented strain recognition, the sensor delivers clear and distinguishable stepwise responses during periodic stretch-release at prescribed strains of 50%, 100%, 150%, and

200%, with stable amplitude gradations between levels and high inter-cycle consistency (Fig. S5 in ESI). This behavior indicates a reliable graded interpretation of strain. Frequency robustness tests show that across different stretching speeds/loading frequencies, the output waveform preserves comparable amplitude and phase features without noticeable distortion or drift (Fig. 4g). Taken together, the PVA/CCB flexible sensor achieves a combined performance of low hysteresis, high sensitivity, and long-term stability through the synergy of reversible crosslinking, conductive-network design, and 3D-printing-guided architecture. This system realizes an integrated structure-function pathway from material to device and provides a high-reliability platform for wearable sensing and precise detection of human motion.

Application of 3D Printed PVA/CCB Hydrogel Strain Sensor

Given the favorable mechanical and sensing properties of the PVA/CCB hydrogel, we deploy it for human motion monitoring (Fig. 5a). Benefiting from low-hysteresis and highly cycle-stable conductive networks, the sensor maintains accurate and repeatable signals under complex dynamic deformations. When attached to the elbow and knee (Figs. 5b and 5c), the resistance exhibits pronounced oscillations during bending and extension, indicating real-time and accurate capture of large-amplitude joint motion. For practical applications, the device also requires a high responsiveness to small deformations. Therefore, we place it on low-strain regions, such as the forehead and chin (Figs. 5d and 5e), and the resistance changes remain clearly discernible under subtle facial or muscle movements, confirming signal resolvability and sensitivity at low strain. Meanwhile, during finger flexion-extension monitoring, the PVA/CCB sensor outputs stable and reproducible step-like plateau signals and exhibits pronounced pulse peaks at the transition moments, demonstrating its capability for the reliable detection of dynamic finger motions (Fig. 5f). Furthermore, we implement the sensor on a robotic finger to demonstrate its practical sensing ap-

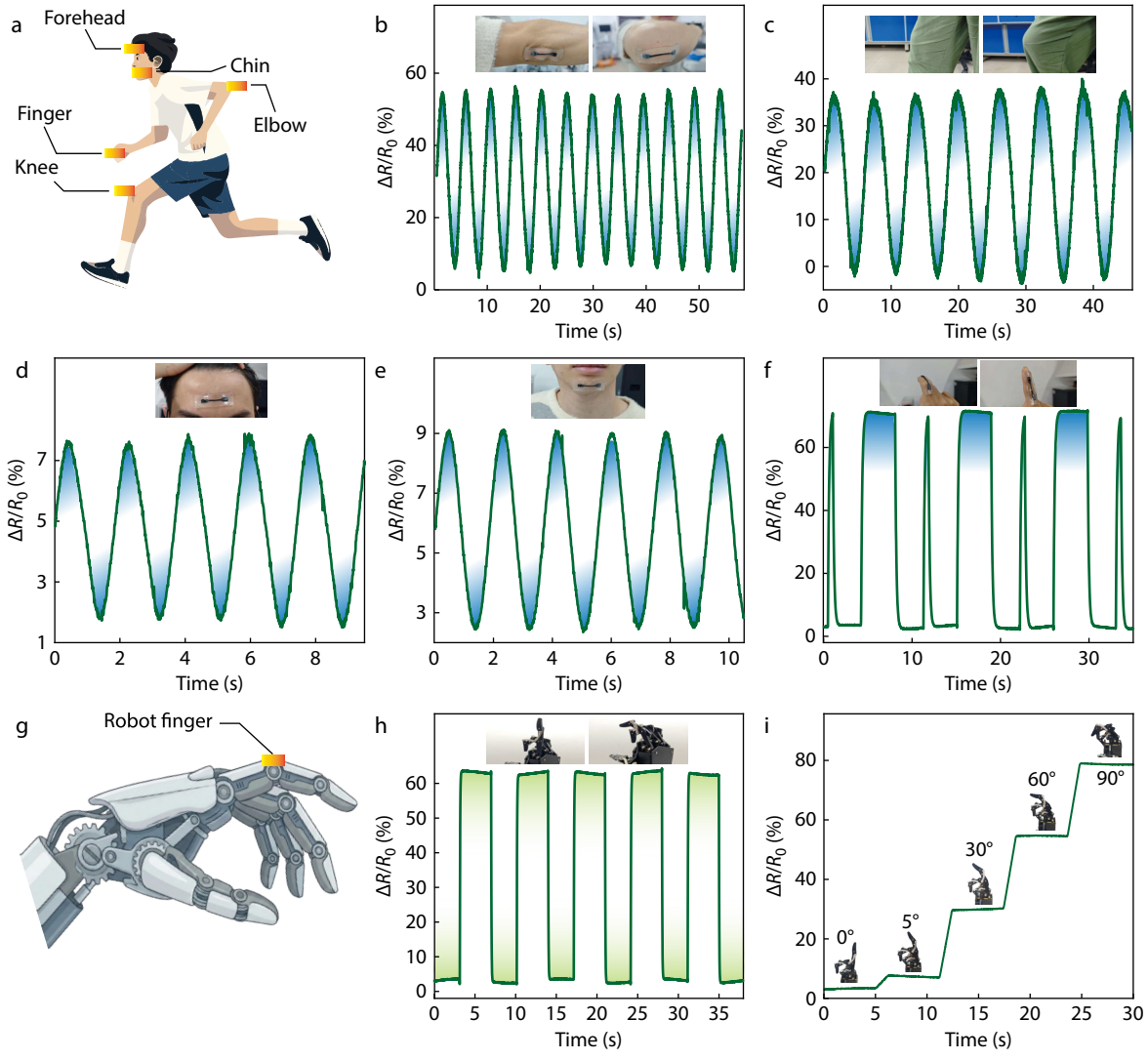

Fig. 5 PVA/CCB strain sensor for human and robotic finger motion monitoring. (a) Schematic illustration of human motion monitoring; (b–f) Applications of the PVA/CCB hydrogel strain sensor in monitoring elbow, knee, forehead, chin, and finger motions; (g) Schematic illustration of robotic finger motion monitoring; (h, i) Applications of the PVA/CCB hydrogel strain sensor in monitoring repetitive bending motions and different bending angles of robotic finger.

https://doi.org/10.1007/s10118-026-3616-7

plication (Fig. 5g). During periodic flexion and extension of the robotic finger, the sensor output exhibits stable and highly reproducible square-wave signals (Fig. 5h), with the signal amplitude and waveform remaining essentially consistent across successive cycles. Moreover, when the robotic finger moves stepwise at different bending angles (0°, 5°, 30°, 60°, and 90°), the relative resistance change of the sensor shows a distinct staircase-like increasing trend (Fig. 5i). The results obtained from the robotic finger demonstrate that the sensor not only identifies discrete motion states but also effectively distinguishes different strain amplitudes, enabling the accurate perception of joint bending angles. This series of applications further underscores the positive role of low hysteresis in terms of signal recovery and waveform fidelity. Collectively, the PVA/CCB flexible sensor delivers sensitive, stable, and repeatable responses across multiple body sites and strain levels, enabling the real-time monitoring of diverse human motions.

During finger motion monitoring, bend-release actions in-

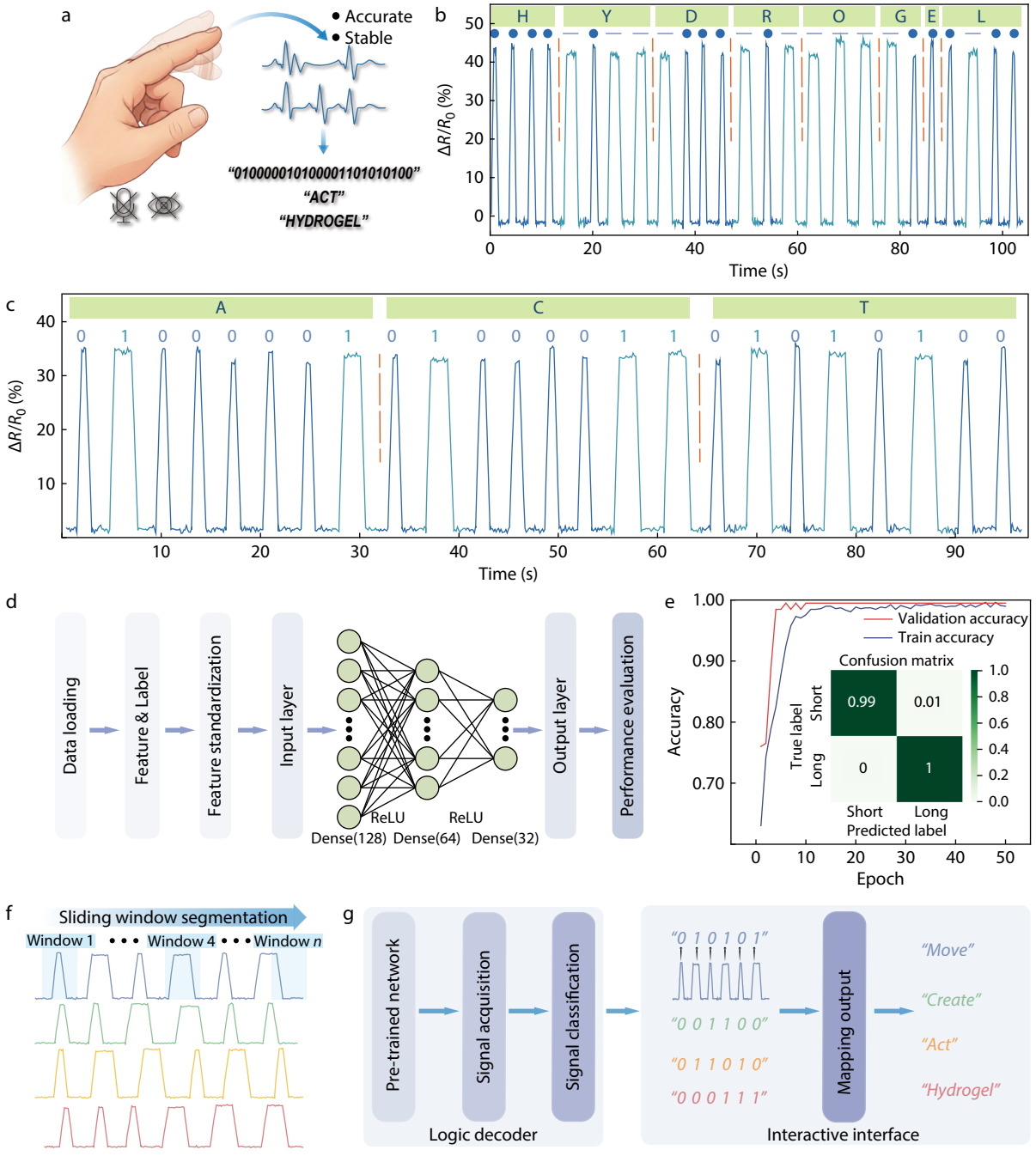

Fig. 6 PVA/CCB strain sensor for intelligent human-machine interaction. (a) Schematic illustration of converting finger motions into stable and distinguishable electrical signals for information interaction; (b) Simulation of the "HYDROGEL" signal; (c) Simulation of the "ACT" signal; (d) Workflow diagram of machine learning neural network; (e) Training performance and results of machine learning after 50 epochs; (f) Continuous strain signals; (g) Classification and mapping results of the interactive system.

https://doi.org/10.1007/s10118-026-3616-7

duce resistance variations. Owing to the accuracy and reliability of the PVA/CCB hydrogel sensor, these variations in resistance enable information interactions (Fig. 6a). The response signatures of the resistance changes can be mapped to Morse code dits and dahs. Rapid bend-release produces short-duration resistance peaks corresponding to dits, whereas a bend with a hold yields sustained resistance changes corresponding to dahs. Based on this principle, we realize a Morse rendering of "HYDROGEL" using sequential finger strains (Fig. 6b). Furthermore, because information in electronic systems is typically transmitted in binary form, the sensor discriminates short and long high-resistance states to represent logical "0" and "1," thereby enabling binary encoding of "ACT" (Fig. 6c).

Building on the foregoing Morse and binary demonstrations, the PVA/CCB hydrogel sensor confirms the precise perception of strain signals with different durations. By leveraging this response feature, we further explore intelligent recognition. To achieve efficient mapping from mechanical strain to electrical signals and accurate discrimination between short- and long-duration high-resistance states, we construct a duration-based dataset and design a three-layer fully connected neural network for classification (Fig. 6d). The model uses ReLU activation and L2 regularization, together with dropout, to suppress overfitting. Benefiting from stable and reproducible outputs under cyclic deformation, the model converges rapidly and maintains a high level of generalization. The classifier achieves 99.49% accuracy for the two categories, and the confusion matrix verifies near-perfect decisions (Fig. 6e). These results indicate that high-fidelity strain transduction enabled by the low-hysteresis conductive network provides stable and separable features for signal-pattern recognition.

The strain signals generated by continuous finger flexion contain richer temporal features (Fig. 6f). Building on stable front-end signals and high-accuracy feature extraction using a machine-learning model, we construct a continuous finger-strain recognition system. The system adopts a sliding time window mechanism to segment real-time signals and perform dynamic encoding. Each segment is independently classified by the neural network and converted into a binary symbol, and the outputs are concatenated temporally to form an instruction sequence. A configurable mapping table establishes the correspondence between binary codes and functions, such as "010101" for Move and "011010" for Launch (Fig. 6g). Users can optimize individual signal boundaries without retraining by adjusting decision thresholds or employing a multi-frame upload strategy, thereby enabling real-time decoding and interaction for complex actions. This human-machine interaction prototype demonstrates a fusion strategy that employs material stability as the foundational layer and intelligent algorithms as the perception layer, providing a practical route towards cognitive and logic-driven applications of flexible sensors in wearable command control, rehabilitation training, and virtual interaction.

CONCLUSIONS

In summary, we develop a 3D-printable PVA/CCB conductive hydrogel that serves as a low-hysteresis sensing platform, establishing a direct connection between the material design and intelligent interaction. By constructing a microphase-separated interlocking network, the PVA/CCB conductive hydrogel synergistically integrates dynamic energy-dissipating bonds with a nano-reinforced framework. This architecture achieves a dynamic balance between energy release and structural recovery, effectively minimizing hysteresis responses and thereby granting exceptional compliance, ultralow hysteresis, and long-term stability to the hydrogel-based strain sensor. Building on this reliable sensing foundation, we further incorporate machine learning to extend its capability beyond simple motion detection, enabling a human-motion recognition system that decodes continuous strain into commands. The integration of stable material performance with intelligent signal processing promotes fluid and trustworthy human-machine dialogue. Therefore, this work not only elucidates the critical role of multiscale low-dissipation structures in designing reliable soft materials but also provides a robust blueprint for next-generation intelligent interactive technologies where signal fidelity is paramount.

Conflict of Interests

The authors declare no interest conflict.

Electronic Supplementary Information

Electronic supplementary information (ESI) is available free of charge in the online version of this article at http://doi.org/10.1007/s10118-026-3616-7.

Data Availability Statement

The data that support the findings of this study are available from the author upon reasonable request. The author's contact information: zly000110@163.com.

ACKNOWLEDGMENTS

This work was financially supported by the National Natural Science Foundation of China (Nos. 82100877 and 52473179), Research Project of the State Key Laboratory of Mechanical System and Vibration (No. MSV202013), Training Program of the Natural Science Foundation of China Youth Fund (No. 20202ZDB01007), the Natural Science Foundation of Jiangxi Province (Nos. 20252BAC200300 and 20252BEJ730346), and the Research Startup Grant of Jiangxi Science & Technology Normal University (No. 2024BSQD15).

REFERENCES

1 Yu, X.; Xie, Z.; Yu, Y.; Lee, J.; Vazquez-Guardado, A.; Luan, H.; Ruban, J.; Ning, X.; Akhtar, A.; Li, D.; Ji, B.; Liu, Y.; Sun, R.; Cao, J.; Huo, Q.; Zhong, Y.; Lee, C.; Kim, S.; Gutruf, P.; Zhang, C.; Xue, Y.; Guo, Q.; Chempakasseril, A.; Tian, P.; Lu, W.; Jeong, J.; Yu, Y. J.; Cornman, J.; Tan, C.; Kim, B.; Lee, K.; Feng, X.; Huang, Y.; Rogers, J. A. Skin-integrated wireless haptic interfaces for virtual and augmented reality. *Nature* **2019**, *575*, 473–479.
2 Sundaram, S.; Kellnhofer, P.; Li, Y.; Zhu, J.; Torralba, A.; Matusik, W.

Graphical Abstract

Hysteresis-free and Fatigue-resistant Conductive Hydrogel Electronics towards Intelligent Human-machine Interaction

Liu-Yu Zhang, Gen Li, Gui-Neng Li, Yu-Zhu Hou, Hua Li, Yu Xue, Wei-Jing Zhao, and Bao-Yang Lu

Nanchang University; Jiangxi Science and Technology Normal University; Shanghai Sixth People's Hospital Affiliated to Shanghai Jiao Tong University School of Medicine; Nanchang Jiaotong Institute

The microphase-separated poly(vinyl alcohol) (PVA)/conductive carbon black (CCB) interlocking hydrogel enables low-hysteresis, high-stability strain sensing for precise motion and gesture monitoring, and, through machine-learning analysis of continuous signals, supports intelligent human-machine interaction.

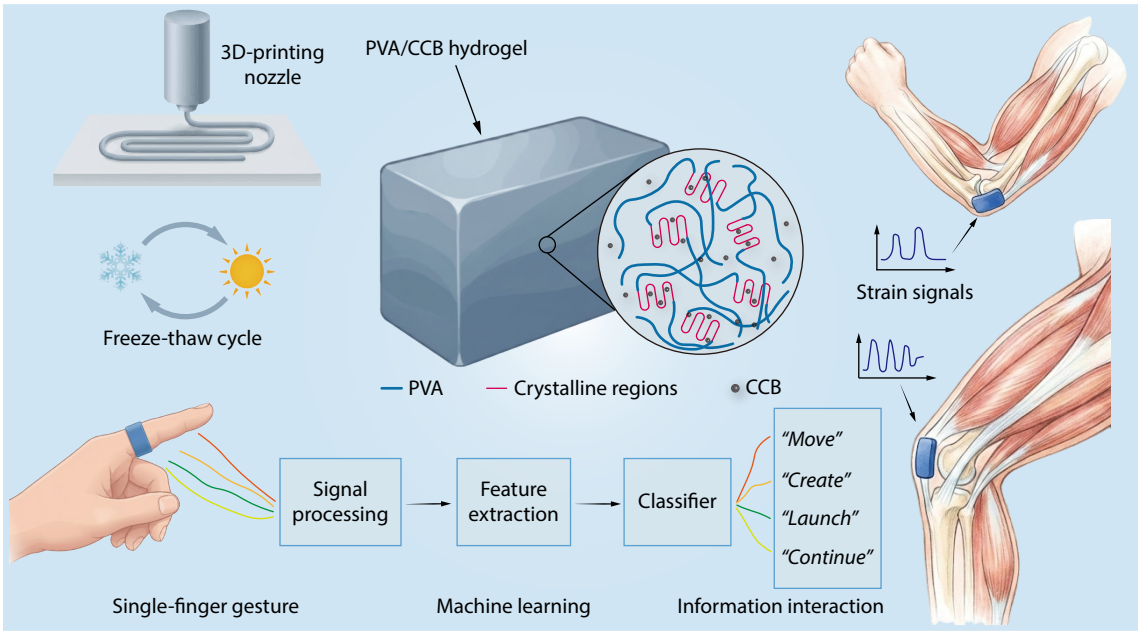

Chinese J. Polym. Sci. 2026, 44, 1830–1842 *https://doi.org/10.1007/s10118-026-3616-7*

Learning the signatures of the human grasp using a scalable tactile glove. *Nature* **2019**, *569*, 698–702.

3 Yin, J.; Li, Y.; Sun, X.; Qin, Z. Tough gelatin-based biogels for wearable sensors. *Soft Sci.* **2025**, *5*, 30.

4 Deng, J.; Wu, J.; Chen, X.; Sarrafian, T.; Varela, C.; Whyte, W.; Guo, C.; Roche, E.; Griffiths, L.; Yuk, H.; Nabzdyk, C.; Zhao, X. A bioadhesive pacing lead for atraumatic cardiac monitoring and stimulation in rodent and porcine models. *Sci. Transl. Med.* **2024**, *16*, eado9003.

5 Hang, C.; Zhao, X.; Xi, S.; Shang, Y.; Yuan, K.; Yang, F.; Wang, Q.; Wang, J.; Zhang, D.; Lu, H. Highly stretchable and self-healing strain sensors for motion detection in wireless human-machine interface. *Nano Energy* **2020**, *76*, 105064.

6 Zhao, Y.; Zhang, S.; Yu, T.; Zhang, Y.; Ye, G.; Cui, H.; He, C.; Jiang, W.; Zhai, Y.; Lu, C.; Gu, X.; Liu, N. Ultra-conformal skin electrodes with synergistically enhanced conductivity for long-time and low-motion artifact epidermal electrophysiology. *Nat. Commun.* **2021**, *12*, 4880.

7 Dong, J.; Peng, Y.; Nie, X.; Li, L.; Zhang, C.; Lai, F.; He, G.; Ma, P.; Wei, Q.; Huang, Y.; Liu, T. Hierarchically designed super-elastic metafabric for thermal-wet comfortable and antibacterial epidermal electrode. *Adv. Funct. Mater.* **2022**, *32*, 2209762.

8 Huang, M.; Liu, S.; Chi, Y.; Li, J.; Sun, H.; Dong, L.; Liu, H.; Liu, C.; Shen, C. Multimodal sensing conductive organohydrogel electronics based on chitosan-encapsulated MXene nanocomposites for deep learning-enhanced ball sports recognition. *Soft Sci.* **2025**, *5*, 24.

9 Zhang, Y.; He, P.; Luo, M.; Xu, X.; Dai, G.; Yang, J. Highly stretchable polymer/silver nanowires composite sensor for human health monitoring. *Nano Res.* **2020**, *13*, 919–926.

10 Markvicka, E.; Bartlett, M.; Huang, X.; Majidi, C. An autonomously electrically self-healing liquid metal-elastomer composite for robust soft-matter robotics and electronics. *Nat. Mater.* **2018**, *17*, 618–624.

11 Wang, L.; Chen, W.; Li, H.; Xu, X.; Zhang, Z.; Wu, L.; Xu, J.; Huang, Y.; Lu, B. Ultrasoft, anti-dehydrated, and highly stretchable carboxymethylcellulose-based organohydrogel strain sensors for non-invasive real-time plant growth monitoring. *Carbohydr. Polym.* **2025**, *364*, 123753.

12 Huang, X.; Zou, J.; Gu, G. Kinematic modeling and control of

variable curvature soft continuum robots. *IEEE/ASME Trans. Mechatronics* **2021**, *26*, 3175–3185.
13 Zhang, N.; Zhou, P.; Yang, X.; Shen, F.; Ren, J.; Hou, T.; Dong, L.; Bian, R.; Wang, D.; Gu, G.; Zhu, X. Biomimetic rigid-soft finger design for highly dexterous and adaptive robotic hands. *Sci. Adv.* **2025**, *11*, eadu2018.
14 Wang, W.; Liu, J.; Li, H.; Zhao, Y.; Wan, R.; Wang, Q.; Xu, J.; Lu, B. Photopatternable PEDOT:PSS hydrogels for high-resolution photolithography. *Adv. Sci.* **2025**, *12*, 2414834.
15 Xue, Y.; Zhang, J.; Chen, X.; Zhang, J.; Chen, G.; Zhang, K.; Lin, J.; Guo, C.; Liu, J. Trigger-detachable hydrogel adhesives for bioelectronic interfaces. *Adv. Funct. Mater.* **2021**, *31*, 2106446.
16 Yao, H.; Yang, W.; Cheng, W.; Tan, Y.; See, H.; Li, S.; Ali, H.; Lim, B.; Liu, Z.; Tee, B. Near-hysteresis-free soft tactile electronic skins for wearables and reliable machine learning. *Proc. Natl. Acad. Sci. U.S.A.* **2020**, *117*, 25352–25359.
17 Zou, J.; Kassim, S. O.; Ren, J.; Vaziri, V.; Aphale, S. S.; Gu, G. A generalized motion control framework of dielectric elastomer actuators: Dynamic modeling, sliding-mode control and experimental evaluation. *IEEE Trans. Robot.* **2024**, *40*, 919–935.
18 Liu, F.; Jing, X.; Yang, J.; Mi, H.; Feng, F.; Liu, Y. Recent progress in low hysteresis gels: strategies, applications, and challenges. *Nano Today* **2025**, *61*, 102601.
19 Huang, B.; Lv, Z.; Zhang, M.; Liu, J.; Liu, H.; Li, T.; Fu, L.; Lin, B.; Xu, C. Low mechanical-hysteresis soft materials: materials, design, and applications. *J. Mater. Chem. A* **2025**, *13*, 15427–15452.
20 Lei, H.; Dong, L.; Li, Y.; Zhang, J.; Chen, H.; Wu, J.; Zhang, Y.; Fan, Q.; Xue, B.; Qin, M.; Chen, B.; Cao, Y.; Wang, W. Stretchable hydrogels with low hysteresis and anti-fatigue fracture based on polyprotein cross-linkers. *Nat. Commun.* **2020**, *11*, 4032.
21 Song, J.; Mou, C.; Balakrishnan, G.; Wang, Y.; Rajagopalan, M.; Schreiner, A.; Naik, D.; Cohen-Karni, T.; Halbreiner, M.; Bettinger, C. Hysteresis-free and high-sensitivity strain sensing of ionically conductive hydrogels. *Adv. NanoBiomed Res.* **2023**, *3*, 2200132.
22 Chen, L.; Jin, Z.; Feng, W.; Sun, L.; Xu, H.; Wang, C. A hyperelastic hydrogel with an ultralarge reversible biaxial strain. *Science* **2024**, *383*, 1455–1461.
23 Sun, X.; Luo, F.; Jiang, F. Low-hysteresis cellulose-based hydrogels for strain detecting. *Macromol. Rapid Commun*. **2025**, *e00521*.
24 Huang, W.; Wang, X.; Luo, F.; Zhao, X.; Chen, K.; Qin, Y. Ultrastretchable, ultralow hysteresis, high-toughness hydrogel strain sensor for pressure recognition with deep learning. *ACS Appl. Mater. Interfaces* **2024**, *16*, 49834–49844.
25 Zhou, L.; Zhao, B.; Liang, J.; Lu, F.; Yang, W.; Xu, J.; Zheng, J.; Liu, Y.; Wang, R.; Liu, Z. Low hysteresis, water retention, anti-freeze multifunctional hydrogel strain sensor for human-machine interfacing and real-time sign language translation. *Mater. Horiz.* **2024**, *11*, 3856–3866.
26 Zhu, R.; Zhu, D.; Zheng, Z.; Wang, X. Tough double network hydrogels with rapid self-reinforcement and low hysteresis based on highly entangled networks. *Nat. Commun.* **2024**, *15*, 1344.
27 Han, S.; Hu, Y.; Wei, J.; Li, S.; Yang, P.; Mi, H.; Liu, C.; Shen, C. A semi-interpenetrating poly(ionic liquid) network-driven low hysteresis and transparent hydrogel as a self-powered multifunctional sensor. *Adv. Funct. Mater.* **2024**, *34*, 2401607.
28 Chen, M.; Qin, W.; Wang, Y.; Zhai, H.; Gu, C.; Zhao, X.; Bi, Y.; Xu, Y.; Ming, Z.; Li, S.; Hu, S.; Zhang, X.; Ma, X.; Yin, S. Dynamic Na^+ bridges: a 3D printing strategy for hydrogels with high strength, low hysteresis, strong adhesion, and self-healing. *Adv. Funct. Mater.* **2026**, 36, e24993.
29 Zuo, F.; Hu, J.; Zhang, S.; Guo, J.; Li, R.; Xin, Y.; Li, C.; Yan, J. Facile preparation of super-strong and tough poly(vinyl alcohol)/carbon nanotube hydrogel enabled by triple crosslinking networks. *Chinese J. Polym. Sci.* **2025**, *43*, 2432–2442.
30 Feng, M.; Yang, D.; Ren, L.; Wei, G.; Gu, G. X-crossing pneumatic artificial muscles. *Sci. Adv.* **2023**, *9*, eadi7133.
31 Xia, J.; He, L.; Lu, Z.; Song, J.; Wang, Q.; Liu, L.; Tian, Y. High performance strain sensor based on carbon black/graphene/ecoflex for human health monitoring and vibration signal detection. *ACS Appl. Nano Mater.* **2023**, *6*, 19279–19289.
32 Liu, R.; Liu, Y.; Fu, S.; Cheng, Y.; Jin, K.; Ma, J.; Wan, Y.; Tian, Y. Humidity adaptive antifreeze hydrogel sensor for intelligent control and human-computer interaction. *Small* **2024**, *20*, 2308092.
33 Adelnia, H.; Ensandoost, R.; Moonshi, S.; Gavgani, J.; Vasafi, E.; Ta, H. Freeze/thawed polyvinyl alcohol hydrogels: present, past and future. *Eur. Polym. J.* **2022**, *164*, 110974.
34 Tavakoli, J.; Gascooke, J.; Xie, N.; Tang, B.; Tang, Y. Enlightening freeze-thaw process of physically cross-linked poly(vinyl alcohol) hydrogels by aggregation-induced emission fluorogens. *ACS Appl. Polym. Mater.* **2019**, *1*, 1390–1398.
35 Zheng, W.; Wang, L.; Jiao, H.; Wu, Z.; Zhao, Q.; Lin, T.; Ma, H.; Zhang, Z.; Xu, X.; Cao, J.; Zhong, J.; Xu, J.; Lu, B. A cost-effective, fast cooling, and efficient anti-inflammatory multilayered topological hydrogel patch for burn wound first aid. *Chem. Eng. J.* **2023**, *455*, 140553.
36 Wang, L.; Wang, W.; Wan, R.; Yao, M.; Chen, W.; Zhang, L.; Xu, J.; Liu, X.; Lu, B. All 3D-printed high-sensitivity adaptive hydrogel strain sensor for accurate plant growth monitoring. *Soft Sci.* **2025**, *5*, 2.
37 Yang, J.; Dong, Z.; Liu, H.; Tian, Y. Bioinspired self-sensing hydrogel actuators: From mechanisms to applications. *Chem. Eng. J.* **2025**, 512, 162743.
38 Chen, G.; Liang, X.; Zhang, P.; Lin, S.; Cai, C.; Yu, Z.; Liu, J. Bioinspired 3D printing of functional materials by harnessing enzyme-induced biomineralization. *Adv. Funct. Mater.* **2022**, *32*, 2113262.
39 Sanandiya, N.; Pai, A.; Seyedin, S.; Tang, F.; Thomas, S.; Xie, F. Chitosan-based electroconductive inks without chemical reaction for cost-effective and versatile 3D printing for electromagnetic interference (EMI) shielding and strain-sensing applications. *Carbohydr. Polym.* **2024**, *337*, 122161.
40 Gao, Q.; Wang, M.; Kang, X.; Zhu, C.; Ge, M. Continuous wet-spinning of flexible and water-stable conductive PEDOT:PSS/PVA composite fibers for wearable sensors. *Compos. Commun.* **2020**, *17*, 134–140.
41 Yu, Y.; Zhou, Z.; Ruan, H.; Li, Y. High conductivity, low-hysteresis, flexible PVA hydrogel multi-functional sensors: wireless wearable sensor for health monitoring. *Chem. Eng. J.* **2025**, *505*, 158877.
42 Li, S.; Xiao, Z.; Yang, H.; Zhu, C.; Chen, G.; Zheng, J.; Ren, J.; Wang, W.; Cong, Y.; Shah, L.; Fu, J. A skin-inspired anisotropic multidimensional sensor based on low hysteresis organohydrogel with linear sensitivity and excellent robustness for directional perception. *Chem. Eng. J.* **2024**, *499*, 156581.
43 Zhao, W.; Chen, L.; Hu, S.; Shi, Z.; Gao, X.; Silberschmidt, V. Printed hydrogel nanocomposites: fine-tuning nanostructure for anisotropic mechanical and conductive properties. *Adv. Compos. Hybrid Mater.* **2020**, *3*, 315–324.
44 Crolla, J.; Britton, M.; Espino, D.; Thomas-Seale, L. The orthotropic viscoelastic characterisation of sub-zero 3D-printed poly(vinyl alcohol) cryogel. *MRS Adv.* **2021**, *6*, 467–471.
45 Niu, R.; Gong, J.; Xu, D.; Tang, T.; Sun, Z. The effect of particle shape on the structure and rheological properties of carbon-based particle suspensions. *Chinese J. Polym. Sci.* **2015**, *33*, 1550–1561.
46 Shen, Z.; Zhang, Z.; Zhang, N.; Li, J.; Zhou, P.; Hu, F.; Rong, Y.; Lu, B.; Gu, G. High-stretchability, ultralow-hysteresis conducting polymer hydrogel strain sensors for soft machines. *Adv. Mater.*

2022, *34*, 2203650.
47 Cao, J.; Zhang, Z.; Wang, L.; Lin, T.; Li, H.; Zhao, Q.; Wang, H.; Liu, X.; Yang, H.; Lu, B. An adhesive, highly stretchable and low-hysteresis alginate-based conductive hydrogel strain sensing system for motion capture. *Int. J. Biol. Macromol.* **2024**, *281*, 136581.
48 Ko, S.; Chhetry, A.; Kim, D.; Yoon, H.; Park, J. Hysteresis-free double-network hydrogel-based strain sensor for wearable smart bioelectronics. *ACS Appl. Mater. Interfaces* **2022**, *14*, 31363–31372.
49 Wei, C.; Wang, Y.; Liang, Y.; Wu, J.; Li, F.; Luo, Q.; Lu, Y.; Liu, C.; Zhang, R.; Lu, Z.; Xu, B.; Qing, N.; Tang, L. Low-hysteresis and highly linear sensors based on environmentally stable, adhesive, and antibacterial hydrogels. *J. Mater. Chem. A* **2024**, *12*, 10392–10402.
50 Peng, S.; Guo, Q.; Thirunavukkarasu, N.; Zheng, Y.; Wang, Z.; Zheng, L.; Wu, L.; Weng, Z. Tailoring of photocurable ionogel toward high resilience and low hysteresis 3D printed versatile porous flexible sensor. *Chem. Eng. J.* **2022**, *439*, 135593.
51 Azadi, S.; Peng, S.; Moshizi, S.; Asadnia, M.; Xu, J.; Park, I.; Wang, C.; Wu, S. Biocompatible and highly stretchable PVA/AgNWs hydrogel strain sensors for human motion detection. *Adv. Mater. Technol.* **2020**, *5*, 2000426.
52 Bhattacharjee, M.; Soni, M.; Escobedo, P.; Dahiya, R. PEDOT:PSS microchannel-based highly sensitive stretchable strain sensor. *Adv. Electron. Mater.* **2020**, *6*, 2000445.
53 Liu, S.; Li, L. Ultrastretchable and self-healing double-network hydrogel for 3D printing and strain sensor. *ACS Appl. Mater. Interfaces* **2017**, *9*, 26429–26437.
54 Zhang, Z.; Chen, G.; Xue, Y.; Duan, Q.; Liang, X.; Lin, T.; Wu, Z.; Tan, Y.; Zhao, Q.; Zheng, W.; Wang, L.; Wang, F.; Luo, X.; Xu, J.; Liu, J.; Lu, B. Fatigue-resistant conducting polymer hydrogels as strain sensor for underwater robotics. *Adv. Funct. Mater.* **2023**, *33*, 2305705.
55 Liu, J.; Chen, X.; Sun, B.; Guo, H.; Guo, Y.; Zhang, S.; Tao, R.; Yang, Q.; Tang, J. Stretchable strain sensor of composite hydrogels with high fatigue resistance and low hysteresis. *J. Mater. Chem. A* **2022**, *10*, 25564–25574.

https://doi.org/10.1007/s10118-026-3616-7